https://doi.org/10.5194/angeo-2020-65
Preprint. Discussion started: 12 October 2020

Annales Geophysicae Discussions

A case study of the spectral parameters of ULF fluctuations before substorms with no evident trigger in the interplanetary space

Nataliya Sergeevna Nosikova[1,2], Nadezda Viktorovna Yagova[2], Lisa Jane Baddeley[3], Dag Arne Lorentzen[3], Dmitriy Anatolyevich Sormakov[4]

[1]National Nuclear University "MEPhI", Moscow, Russia
[2] Schmidt Institute of Physics of the Earth of the Russian Academy of Sciences (IPE RAS), Moscow, Russia
[3]University Center on Svalbard, Norway
[4]Arctic and Antarctic Research Institute, AARI, Geophysics department, Sankt-Petersburg, Russia

Correspondence to: Nataliya S Nosikova (NSNosikova@mephi.ru)

Abstract. Our recent study (Yagova et al, 2017) shows that ultralow frequency (ULF) pulsations are seen in ground-based magnetic and luminosity data in the polar cap for a few hours preceding isolated non-triggered substorms. Such pulsations are characterised by a high level of coherence. There might be two possible origins of these pulsations: ULF disturbances in the solar wind or processes inside the magnetosphere, which lead to a substorm generation. In this case, the first scenario should be considered as a substorm trigger. To understand the role of the mentioned mechanisms in developing of pulsations, a detailed case study has been carried out. It is shown that before a weak substorm, fluctuations with the central frequency 1.5 mHz are observed in the both polar caps in ground-based geomagnetic data. Coherent pulsations with the same main frequency are also seen in the magnetotail magnetic field, in addition to simultaneous electron concentration in the ionosphere, while fluctuations in electron temperature and electron flux in the magnetosphere have a slightly different main frequency. These pulsations appeared after ULF activity in solar wind and interplanetary magnetic field became inappreciable.

1 Introduction

Substorms are a spectacular phenomenon, which occur in the near Earth space, which have been studied for more than 50 years. A substorm is essentially a rapid energy release in the magnetotail, which is recorded as a local change in the geomagnetic field in the night sector at high latitudes and is accompanied by auroral luminosity brightening. Usually, the mean threshold value for a geomagnetic bay is a few hundred nT and a threshold is defined as 100 nT. Such a value is comparable with magnitude of global ULF pulsations, which are resulting from magnetic closed field-line resonance. ULF activity is also observed in the polar caps, but oscillations are specified by lower amplitudes, and the central frequency ~ a few mHz (Bland, 2016). These pulsations are simultaneously seen in geomagnetic and radar data and might be a result of internal processes in the magnetosphere; be directly driven by perturbations in the Solar Wind (SW) or related to substorms (see references from introduction by Bland, 2016).

https://doi.org/10.5194/angeo-2020-65
Preprint. Discussion started: 12 October 2020

Annales Geophysicae Discussions

In view of this, substorms and ULF activity are important processes in magnetospheric dynamics. Akasofu 2017 summarises the current understanding of substorms and provides a list of controversial topics. One of them is a substorm developing without any evident external (i.e. from the Solar Wind / Interplanetary Magnetic Field (IMF)) trigger (a so called non-triggered substorm, see introduction Yagova et al, 2017).

As it was shown in (Yagova et al, 2017), geomagnetic and auroral luminosity ($\lambda = 557.7$ nm), the specific pre-substorm pulsations in the frequency range 1-5 mHz (Pc5/Pi3) are observed in the polar cap for a few hours, preceding an isolated non-triggered substorm. The parameters quantifying their spectral content and spatial scale differ from those for typical polar cap Pi3s. The study raises a number of questions. First of all, do these pulsations have an extra-magnetospheric origin (Kepko et al., 2002) or do they develop inside the magnetosphere? To discriminate between these possibilities and extend the physical understanding of these oscillations, a case study investigating the hours preceding a non-triggered substorm is carried out in the present paper. A comparison is made between spectral parameters for fluctuations in the IMF, SW, in the magnetotail (using satellites data) as well as in ground-based measured geomagnetic field in both hemispheres and the electron density in the ionosphere. Interrelation between pulsations in different regions is studied quantitatively, using power spectra density (PSD), spectral coherence, and correlation between spectral power variations.

The present study is focused on one event (08.08.2007); which was recorded at an auroral magnetometer station with a quiet background. The Dst index for the previous 4 days indicated quiet geomagnetic activity with a maximum value of -50nT. For 6 hours preceding the substorm, the SW and IMF stayed moderate and undisturbed (see fig.2 and section 3.1 for details). The studied substorm can also be classed as isolated, since the maximum value of AE did not exceed 80 nT for at least 3 previous hours. The substorm perfectly fits in the dataset of selected days used in the paper (Yagova et al, 2017). According to that paper, it is expected to see specific pre-substorm ULF pulsations recorded during several pre-substorm hours, that are studied for this event together with fluctuations in the magnetotail, recorded by Cluster satellites. Pulsations in the SW and IMF are also examined.

2 Data processing

2.1 Data

Data from the IMAGE magnetometer network, Vostok, DVS, DRV, THL magnetic stations, EISCAT radar, CLUSTER, DMSP as well as OMNI Solar wind and IMF data were utilised. Clusters' positions and their projections on the map together with stations' locations are given in Figure 1.

IMAGE is a European magnetometer network equipped with three-component flux-gate magnetometers with 10 s initial time resolution (Tanskanen, 2009). The chain is located approximately along the magnetic meridian 100 (MM100), and it covers CGM latitudes from Φ=77° to 40°. Information on the stations utilised in this study and their coordinates is presented in Table 1.

https://doi.org/10.5194/angeo-2020-65
Preprint. Discussion started: 12 October 2020


Annales Geophysicae Discussions

The EISCAT Svalbard radar (ESR) is co-located with the LYR magnetometer station (Φ=75.4°) and can make detailed measurements of ionospheric electron density, electron temperature, ion temperature and ion line-of-sight velocity. The radar operates in the 500 MHz band with a peak transmitter power of 1000 kW. In the present paper, data from the 42-meter dish taken during the International Polar Year (2007–2008) are used.

To map the magnetic field variations from the magnetotail to the ground, data from Cluster satellites fluxgate magnetometer have been included (Balogh et al., 1997). The values of footprint coordinates are taken from https://sscweb.gsfc.nasa.gov/cgi-bin/Locator.cgi. The Tsyganenko 89C model is used for field line tracing

On the 8th of August 2007 (day 220) all four Cluster satellites were located in the southern tail lobe at radial distances of between 15 to 20 Re. Specifically, fluxgate magnetometer data from Cluster 1 and 3 are used (which had a separation distance of approximately 1Re along the Sun-Earth line). Using the TS01 model, Cluster 3 was nearly conjugated with the DRV station (its southern footprint at 17:10 UT was at -68.7°, 141.4° geographic and -76°, 236° CGM).

2.2 Data Processing

Preliminary data processing for magnetic data includes low-pass filtration and decimation to a common 1-minute temporal resolution and rotation to a field-aligned system. For the ground stations, the notations B_N and B_E are used for the components oriented northward along the magnetic meridian, and eastward (orthogonal), respectively. In the case of the magnetospheric satellite measurements of the magnetic field, a local field-aligned system is used. For each time instant, there are two magnetic field vectors in GSE coordinate system, i.e. the instantaneous vector **B** and the averaged over the time window one $\mathbf{B}_{av}$. The field aligned component $B_{||}$ is defined as a projection of **B** to $\mathbf{B}_{av}$. The radial component B_ρ is normal to $\mathbf{B}_{av}$ and lies in the plane containing **B** and the Earth centre and directed downward. The azimuthal component B_r is normal to both $B_{||}$ and B_ρ: its direction is determined from the condition that three components form a right-hand triangle. Electron concentration registered by the EISCAT radar are preliminarily sliced with height, averaged, and passed through the low-band filter with a cutoff frequency f_c=8.3 mHz. In fact, 8th of August relates to the polar-day on Svalbard while level of solar-radiation is high. Nevertheless, variations of electron density (ΔNe) are suitable for analysis.

The processing of all data (ground and space based instruments) to a common temporal resolution allows a cross-spectral analysis to be performed between the various data sets. The Blackman-Tukey method (Kay, 1998) is applied to obtain a power spectra density (PSD) for each variable, and spectral coherence and phase difference for each pair of variables. The spectra are calculated in a 96-points (5760 s) sliding window with an 8-min shift between subsequent intervals.

To quantify a shape of a PSD spectrum, the coefficients L_i of the expansion of σ(F) dependence into Lejendre series were used, where σ=log(PSD) is and F=log(f) (Yagova et al., 2007; 2010). As it was shown in Yagova et al., 2017, the parameter Q=-L_2 is higher for pre-substorm pulsations, than for the typical polar cap Pi3s. Enhanced Q values correspond to a maximum of a "whitened" spectrum near the F-band central value. So that, Q parameter is one of the important characteristics to look at.

OMNI data (time delayed to the Bow Shock) are used for spectral estimations in the IMF whilst Cluster data are used for the magnetotail. Various studies have looked at the response time of the magnetosphere to changes in the Solar Wind (primarily

https://doi.org/10.5194/angeo-2020-65
Preprint. Discussion started: 12 October 2020


Annales Geophysicae Discussions

to changes in the IMF). Wing et al. 2002 found a the nightside response time to changes in the IMF of ~12 mins (at geosynchronous orbit). Given that this study is looking at pulsations with a periodicity of ~12 minutes (1.5 mHz) and using a 1.5-hour sampling window for PSD and coherence estimates then the OMNI data has not undergone any additional time lag when evaluating the coherence between that and the Cluster data.

3 Results of the analysis

3.1 Non-triggered substorm on day 220 2007 and space weather conditions

A weak substorm, registered at 20:30 UT on 8th of August 2007 (Day 220) at TRO station is studied in detail. The magnetic field data from the TRO and BJN stations and AE-index, as well as IMF and SW parameters are shown in Figure 2, left panel. It is seen from the Figure, that the IMF was undisturbed, indicating no features which could be considered as a substorm trigger, and the absolute value of the Bz component hardly exceed 3 nT. The absolute value of the Vx component was slightly decreasing for the entire period and the mean value was about 500 km/s, which corresponds to moderate SW. The SW Dynamic pressure stayed low and there were no rapid changes, which can be considered as an external substorm trigger. The AE index was increasing from 14 UT to 16 UT and there were two enhancements: around 17 UT, and at 20:30 UT. The second enhancement, at 20:30 UT, marked with the vertical blue arrow, corresponds to the substorm studied. Although the magnitude of the substorm bay is small (~100 nT), observations by DMSP-satellite (F16, Figure 2b, top right panel) indicate auroral enhancements consistent with a substorm (i.e. particle precipitation occurring from the magnetotail). It should be noted that even if the first enhancement at 17 UT relates to a substorm activation, it does not break the criteria required for the second substorm to be considered isolated. It also should be added, that there is no ground based optical observations available in the high latitude northern region due to 24-hour daylight conditions in northern Scandinavia.

3.2 ULF fluctuations on the ground and in space

3.2.1 Geomagnetic pulsations on the ground. Northern hemisphere

As was mentioned above, it is expected to find Pc5/Pi3 pulsations, similar to pre-substorm pulsations (Yagova et al., 2017), in the polar cap before the studied substorm. Indeed, ULF pulsations are observed in the ground magnetometer data stations located on Svalbard (from NAL to HOR) and at BJN and become indistinct at TRO station, situated on the mainland (Figure 3). The time series starts at 15:10 UT and stretches for 180 minutes. The maximal amplitude reaches ~25 nT peak to peak at ~16:30 UT (t=80 min) for LYR and NAL and then decreases for the value of a few nT. Even though the pulsations have small amplitude, they continue for long time.

The diurnal variations of the Pi3 (1-4 mHz) power at NAL is controlled by two active regions: the polar cusp, which is responsible for near-noon activity, and the polar boundary of auroral oval in the morning and evening MLT sectors (see Yagova et al. (2004) for details). The station crosses both zones at different UTs with a dependence on seasons and geomagnetic

https://doi.org/10.5194/angeo-2020-65
Preprint. Discussion started: 12 October 2020

activity in the morning and afternoon MLT sectors. The PSD variation during the day analysed is shown in Figure 4(a). Each data point along the time axis in Figure 4 (b) corresponds to a starting point of a 1.5-hour interval. After the cusp-related maximum near MLT noon (UT=9) (indicated by the vertical red arrow), the PSD reaches a maximum at 13 UT (16 MLT) (indicated by the vertical purple arrow). Afternoon Pi3s seen after 15 UT do not relate to the cusp activity and are the object of our special interest.

To clarify, how the contribution of polar cap and auroral oval activity to the NAL pulsations changes with time, the variation of the Pi3 PSD ratio, R, and spectral coherence for THL-NAL and HOR-NAL station pairs are given on right (Figure 4, b-c). HOR is located ~ 3 degrees southward from NAL on the MM100 chain, while THL lies at Φ=84.84°, i.e. deep in the polar cap. Although THL is shifted by 5.5 hours in MLT from the MM110 stations, the diurnal variation is almost negligible for this location (Yagova et al., 2010) and this station can be taken as an indicator of condition in the polar cap. As it was shown (Yagova et al, 2017), the main part of the pulsation power is concentrated in the frequency band from 1.25 to 1.9 mHz, and UT from 8 to 20, i.e. from pre-noon to almost midnight in MLT. It is seen from the Figure 4b, both THL/NAL and HOR/NAL PSD ratio lie below 1 at near-noon hours, i.e. NAL is dominating, probably due to cusp-related activity. From 11 to 16:30 UT, the THL/NAL spectral ratio exceeds 1, while HOR/NAL spectral ratio almost equals 1, i.e. the PSD deep in the polar cap is maximal. Then the HOR/NAL PSD ratio grows while the THL-NAL PSD ratio stands at 1. From 13 to 17 UT, the pulsations are coherent for both the THL-NAL and HOR-NAL station pairs with coherence maxima at 14 and 16 UT (Figure 4c). For the first maximum, the HOR-NAL spectral coherence is higher, while for the second one the coherence for the THL-NAL station pair exceeds that for HOR-NAL. Thereby, after 15 UT, the polar cap (THL) pulsations demonstrate both the highest PSD and coherence with those at NAL. This effect can be associated with NAL moving from the auroral oval to the polar cap or can also result from time variations of pulsation properties in space.

An example of the B_N component variations and their spectral parameters are presented in Figure 5. The time series start at 15:44 UT and stretches for 90 minutes. The peak-to-peak amplitude is about 25 nT at NAL and THL, and it is ~15 nT at HOR. The main maximum of PSD at all the stations is found at f_1=1.5 mHz (~11 minutes), and the value of the PSD decreases with CGM latitude from THL to HOR (Figure 5b). This spectral coherence for both the NAL-THL and the NAL-HOR station pairs also demonstrate a maximum at $f = f_1$ (Figure 5c). Note, that the spectral coherence between NAL and THL (green line in figures 6c and 6d) is higher, than between NAL and HOR (blue line in Figures 5, c, d). The pulsations at NAL and THL are almost in phase in the vicinity of f_1 frequency, while the phase changes at about π between NAL and HOR. Similarly, to the pre-substorm pulsations analysed in (Yagova et al., 2017), the pulsations in the polar cap are characterised by a clear spectral maximum, and, the only visible difference from typical auroral Pc5s, is a lower frequency of the main maximum (f_1=1.5 mHz).

3.2.2 Magnetic pulsations in the magnetotail and IMF

In (Yagova et al., 2017), two possibilities for the development of a substorm with no clear external trigger in non-wave parameters of the interplanetary space were discussed. If the first scenario is realised, a substorm is, in fact, externally triggered, but then fluctuations in mHz frequency range in the interplanetary medium should be added to the usual set of trigger

https://doi.org/10.5194/angeo-2020-65
Preprint. Discussion started: 12 October 2020


Annales Geophysicae Discussions

parameters. Under the second scenario, a purely non-triggered substorm develops due to inner processes in the magnetosphere. To discriminate between these two possibilities, ULF disturbances in the SW and the magnetotail were analysed.

The average spectral power and coherence of magnetic field fluctuations in the IMF, calculated from OMNI, and in the magnetotail, recorded by Clusters 1 and 3, are presented in Figure 6 (over the same frequency range, 1.2–1.9 mHz, as those presented in Figure 4). The variations in spectral power of the three IMF components and field aligned component $b_{\parallel}$ in the magnetotail (Cluster3) are given in Figure 6a. One can see from the Figure, that the spectral power in the IMF decreases rapidly at about 13.30 UT (black, dashed arrow in the Figure), and then about 15 UT the decrease is seen in the magnetotail. Simultaneously, the coherence between pulsations, as measured by Cluster 3 and Cluster 1, in the magnetotail (Figure 6b) jumps almost to unity, while no severe changes in IMF-Cluster coherence occur. In the coherence panel, only X-component of IMF is shown. The coherence variations between Cluster field aligned and Y and Z IMF components are similar to Cluster – b_x coherence. However, the latter demonstrates a closer agreement to the coherence variations within the magnetotail before the pulsation regime changed at about 15 UT (magenta curve in Figure 6b). The change of pulsation regime in the magnetotail is rather steep and it can be seen in the time domain as well. Figure 7 shows the pulsations in $b_{\parallel}$ registered simultaneously at Clusters 1 and 3 and their PSD spectra. The time series for the interval started at 15:04 UT is given in Figure 7a. The switch from moderate coherence to almost identical pulsations is seen at about 15:30 and marked with an arrow. The PSD spectra for the interval started at 15:44 (Figure 7b) has the main spectral maximum at f=1.5 mHz, i.e. at the same frequency f_i, as on the ground.

The characteristics of the magnetotail are more sensitive to the polarization parameters of the pulsations (in comparison to a simple amplitude based investigation) (Pilipenko et al., 2013). Let us consider how spectral shape and polarisation of the magnetotail pulsations change during the day. The results for the Q-parameter and polarisation for Cluster-3 are given in Figure 8. Q growth starts immediately after the switch off of mHz fluctuations in the interplanetary space (dash-dot arrow at about 13.5 UT) and it reaches maximal value at 15 UT and then remains high until 18 UT. This effect is seen both in field aligned and transversal components. For $b_{\parallel}$, Q slowly fluctuates between -0.5 and 0.5 from 0 at 13 UT and afterwards reaches almost 1 within half an hour. The growth for the transversal components is not so quick, and the Q-factor reaches its maximal value after 15 UT. For this time interval, the maximal Q values are found for the b_{ρ} component. The wave polarisation is also changing during the interval analysed as it is seen from the variations of the spectral power ratio, R and phase difference, $\Delta\varphi$ for the $b_{\parallel}$-b_{ρ} and the $b_{\parallel}$-b_{φ} component pairs (Figure 8, b, c). For both pairs of components, R exceeds unity almost all day long, i.e. the compressional component is dominating. The only exceptions are registered at 3, 8, and 15 UT. In the afternoon MLT sector, i.e. after 9 UT, it first increases from 2 to nearly 10 and then drops to 2 for the $b_{\parallel}$-b_{ρ} and below unity for the $b_{\parallel}$-b_{φ} component pairs. Its average values during the 15-18 UT interval are 2-3 times lower than for the previous 3 hours. Averaged over the same frequency band, the sin of the inter-component phase difference, $\Delta\varphi$, is shown at the bottom panel. Before 15 UT, the parameter varies predominantly in the interval [-0.5, 0.8] and it differs for two component pairs. At 15 UT it changes to almost unity for both component pairs. This corresponds to $\pi/2$ phase difference between field aligned and each of

https://doi.org/10.5194/angeo-2020-65
Preprint. Discussion started: 12 October 2020


Annales Geophysicae Discussions

transversal components. The interval of π/2 phase difference and low R values are seen in Figure 8 from 15 till 18 UT, i.e. it coincides with the interval of low amplitude, high Q and spectral coherence of Pi3 pulsations in the magnetotail

3.2.3 ULF waves in the magnetotail and on the ground. Inter-hemispheric relation

Since the Cluster spacecraft was in the southern tail lobe, only a footprint in the Southern polar can be calculated. However, coherent Pi3 pulsations are regularly registered in the two hemispheres (see, for example, Fraser-Smith, 1982). To understand, how the magnetotail pulsations are related to those recorded in the two polar cap ionospheres, the pulsations recorded at Cluster have been compared with those, recorded in the Southern Polar cap, and the latter with the Northern polar cap pulsations. A time series of the pulsations registered simultaneously in the magnetotail at Cluster 3 and in both polar cap ionospheres are presented in Figure 9 (*a-c*) and the spectral coherence for the pairs of components with maximal coherence at the f_1 frequency are given in panels (*d-f*). Pi3s at the DRV station, which is nominally conjugated with Cluster-3, have a peak-to-peak amplitude of about 2 nT (Figure 9*a*), and the maximal coherence, γ^2, at 1.5 mHz exceeds 0.9 for both field-aligned and transversal components (Figure 12*d*). It is the maximal value among all the satellite-ground pairs. Pulsations at the VOS station, located deep in the southern polar cap, are similar to the pulsations at Cluster-3 and at DRV. Their peak-to-peak amplitudes reach 4 nT (Figure 9*b*), and Cluster3-VOS coherence near the frequency f_1 $\gamma^2 \approx 0.7$ (Figure 9*e*). At VOS the field-aligned component in the magnetotail is higher than that with transversal components. During this interval, the ground Pi3s are more intensive in the Northern than in the Southern hemisphere. Hence, the peak-to-peak amplitude at NAL is about 25 nT (Figure 9c). The maximal coherence between the NAL and Cluster pulsations is found for the b_p-b_N component pair and approximately equals to 0.9 (Figure 9*f*). The results show that there is a high coherence of pulsations in the magnetotail and in the polar cap ionospheres between 15:44 and 16:14 UT.

The time evolution of spectral power and coherence for all possible pairs of components for Cluster 3 and VOS is presented in Figure 10. The VOS station is taken, because it is located in the polar cap at any local time, and the influence of cusp and auroral activity is minimal for it. A decrease of spectral power at VOS starts immediately after the "switch off" of IMF fluctuations (this instant dash-dot arrow in Figure 10). However, the total decrease of spectral power in the ionosphere is not so severe as in the magnetotail. As a result, the tail to ground (T-G) spectral power ratio $R_{T\text{-}G}$ during the interval 15-18 UT is high in comparison with the previous hours (Figure 10b). The spectral coherence is also higher than its average value during the day, especially for the $b_{||}$ (Cluster)- b_N (VOS) component pair (Figure 10c).

The evolution of averaged spectral coherence between Cluster 3 and 4 ground-based stations in the both hemispheres is shown in Figure 11. The DRV station is nominally conjugated to Cluster-3, NAL station is located in the Northern hemisphere, at the substorm meridian, VOS and THL are placed deeper in southern and northern polar caps respectively as it was mentioned above. Three columns of the Figure 11 correspond to the three magnetic field components in the magnetotail, and four rows to the four stations. The two ground horizontal magnetic components are colour coded with b_N in green and b_E in orange. The time interval from 8 to 20 UT corresponds to hours from local noon to midnight at the substorm meridian and includes the

https://doi.org/10.5194/angeo-2020-65
Preprint. Discussion started: 12 October 2020


Annales Geophysicae Discussions

interval from 13 to 18 UT, i.e. from the switch-off of the IMF ULF activity until last pre-substorm hours. The highest coherence is found for the b_N (DRV)-b_φ (Cluster-3) component pair and last for 2 hours from 15 to 17 UT. During the interval, a large-scale pulsation with a high fraction of transversal (Alfven) components in total spectral power is recorded in the magnetotail. A high (γ^2=0.7) but short coherence maximum is seen also in b_N (DRV)-$b_\parallel$ (Cluster-3) component pair. A similar to b_N (DRV)-b_φ (Cluster-3) time evolution is found for the b_E (VOS)-$b_\parallel$ (Cluster-3) and b_E (VOS)-b_φ (Cluster-3) component pairs, but at somewhat lower absolute values of γ^2. As it is seen from the bottom two rows of panels, during the 15-17 UT time interval, the averaged coherence hardly exceeds 0.5 for all components Cluster 3 - NAL and Cluster 3 - THL, i.e., for stations, located in the Northern polar cap. Generally, the averaged coherence between magnetotail Pi3s with northern polar cap ones is lower than that for the Southern polar cap.

However, the inter-relation between the pulsations in the polar caps cannot be completely described by their spectral coherence with the only a single location on open field lines, in the magnetotail. It seems possible to partly compensate this with the analysis of the coherence between the two polar caps and within each cap. Since the ionospheric observations are available in the Northern hemisphere at the NAL longitude, all possible pairs of horizontal components for two combinations of stations VOS-DVS in the Southern hemisphere, and DVS-NAL between the two hemispheres were analysed. It should be noted, that the maximal coherence at high latitudes is possible not only for the corresponding components (Lepidi et al., 1996). Hence, a maximal coherence can be found for two polar cap stations not between both meridional components, but between e.g. meridional component at the first station and latitudinal component at the second station. The results for the 8-20 UT are given in Figure 12. A high coherence (γ^2>0.5) is seen between the b_N component at VOS and b_E at DVS (Figure 12a) and between the b_E component at VOS and both DVS horizontal components for the 15-18 UT interval (Figure 12b). As for inter-hemispheric coherence for the same time interval, it is maximal for the b_N component at both DVS and NAL (Figure 12c).

The results of coherence analysis between the magnetotail and ground Pi3 and in the two polar caps on Earth show that the Pi3 pulsation recorded after 15 UT is characterised by the high coherence. To speculate on the interrelation between pulsations at different locations, it might be summarised as following:

1) A compressional/shear Alfven wave in the magnetotail is propagating predominantly in transversal/field aligned directions, respectively. A high coherence between the pulsations observed by ground magnetometers in each polar cap demonstrate that these waves exist in both tail lobes.

2) This leads to coherent pulsations in both polar caps with a higher coherence between the meridional components for nominally conjugated positions and a higher cross-component coherence for the pulsations inside the Southern polar cap.

https://doi.org/10.5194/angeo-2020-65
Preprint. Discussion started: 12 October 2020


Annales Geophysicae Discussions

3.2.4 Electron density fluctuations in the ionosphere

To examine electron density fluctuations in the ionosphere for different altitudes EISCAT radar data have been used. The background Ne level was high due to Solar Extreme Ultraviolet (EUV) ionisation but application of a low-bound filter (see sect. 2.2) allows to take into consideration only fluctuations of electron density ΔNe for each altitude.

An example of pulsations and their PSD and coherence spectra at 15:44, registered in the b_N component of magnetic field at NAL and electron density variations Ne in the altitude band centred at h=205 km is given in Figure 13. Similarity of both signals is clearly seen even from the time series (Figure 13*a*), and it is also expressed in the common spectral maximum at f_i=1.5 mHz (Figure 13*b*) and in a wide coherence maximum with $\gamma_{max}\approx 0.9$ (Figure 13*c*). Pulsations are reverse-phase, as is clearly seen from both time series and the phase-difference, which is nearly π at f_i frequency (Figure 13*d*).

Time variation of γ^2 altitude dependence is given in Figure 14 (a) for the 15:30-18 UT interval in the frequency band 1.2-1.9 mHz, (in the vicinity of f_i frequency). Before 16:30 UT, the highest integral coherence is registered with maximum at about 200 km. The same altitude of maximal coherence is seen from 16:40 until 17:30 UT. Besides, several spots of high coherence were found at lower (~150 km centred at 17 UT) and higher (350 km around 16:30 UT and 420 km at 17-17:30 UT) altitudes. An altitude profile taken at 15:44 UT is shown in Figure 14b. Spectral coherence is high ($\gamma^2 > = 0.5$) in the altitude range from 120 to 350 km, and the maximal coherence is found at h=205 km. High coherence between geomagnetic and Ne pulsations can be a result of modulated particle precipitation. The altitudes where the highest coherence is found, correspond to hundreds of eV energies of penetrated electrons.

3.2.5 Summary

To summarise the observational results:

- Geomagnetic field pulsations during a few hours preceding a weak isolated non-triggered substorm on Day 2007 220 were registered in both the Northern and Southern polar caps
- Such pulsations are also observed in the tail and characterised by a high coherence with the pulsations on the ground
- The pulsations are seen simultaneously in the ionospheric electron density enhancements in the Northern Polar Cap.

4 Discussion and Conclusion

An isolated non-triggered substorm on August 8, 2007 (DAY 2007 220) at 20:30 UT at MM100 occurred during a period of IMF parameters, typical for non-substorm intervals. The amplitude of the IMF fluctuations in the Pc5-Pi3 (1-5 mHz) frequency band decreased significantly at 13:30 UT (Figure 6b). Observations made in the magnetotail (by Cluster) and in the polar cap ionosphere (by ground magnetometers and the EISCAT radar) indicate that, at the same time, the Pc5/Pi3 ULF characteristics in this region changed. A most impressive feature of the pulsations in the magnetotail during the last pre-substorm hours is a

https://doi.org/10.5194/angeo-2020-65
Preprint. Discussion started: 12 October 2020

Annales Geophysicae Discussions

high Q factor, with a central frequency about 1.5 mHz and extremely high coherence between the two Cluster satellites. The visible pulsations are almost in-phase. At the same moment the contribution of b_ρ and b_φ components to the total spectral power increases (these are the components, transversal to the main magnetic field B). The pulsation is also recorded in both polar caps by ground magnetometers. Coherence analysis shows that the maximal coherence is found for nominally conjugated positions in the magnetotail and in the southern polar cap ionosphere and between the two hemispheres for the transversal magnetic field components in the magnetotail and the b_N in the ground magnetometer data, while for non-conjugated position it the same hemisphere the coherence is higher for the field-aligned component in the magnetotail and b_E in the ground magnetometer data. This could mean that the wave is a combination of a compressional mode and shear Alfven modes contributing predominantly to wave transport in transversal and parallel direction to **B**, respectively. This pulsation is also characterised by high coherence of geomagnetic Pi3 pulsations in the both polar caps with variations of electron concentration in the northern polar cap ionosphere.

These results, although found in the case study, can be important, as they allow formulating a hypothesis about factors, which can be favourable for substorm development without any classical external trigger. Rather paradoxically, the decrease of extra-magnetospheric fluctuations in the 1-5 mHz frequency range coincides in time with change of ULF regime in the geomagnetic tail. Although Pc5/Pi3 amplitudes are almost the same, the spatial scale of pulsations grows essentially, and similar variations are seen in the geomagnetic field both in the polar caps and in the conjugated regions in the magnetosphere and in the geomagnetic tail.

This is a case study, so more data are needed to build up a statistically significant confidence in our proposed hypothesis, outline below:

1. Even if IMF fluctuations at mHz frequencies is included in an analysis of possible external substorm triggers, a substorm can develop under IMF/SW parameters typical for non-disturbed days.
2. Pc5/Pi3 pulsations in the geomagnetic tail and in the polar caps might play some role in the development of a non-triggered substorm. They can be either an indicator (precursor), or an active agent in substorm preparation
3. Pre-substorm Pc5/Pi3 pulsations are characterised by relatively small amplitudes along with extremely large spatial scale. They have some spectral features which are untypical for open field lines, i.e. relatively narrow Pc-like spectra and a higher fraction of the transversal components in the total spectral power. These pulsations are seen simultaneously in the magnetic field and in electron density in the ionosphere.

Data availability: Publicly available ground-based magnetometer data: IMAGE through https://space.fmi.fi/image/www/, INTERMAGNET through www.intermagnet.org. Magnetometer data from VOS station are available through (http://geophys.aari.ru) upon request. EISCAT data are publicly available through https://www.eiscat.se/scientist/data/. Cluster

https://doi.org/10.5194/angeo-2020-65
Preprint. Discussion started: 12 October 2020

Annales Geophysicae Discussions

and OMNI data are publicly available through CDAWEB (https://cdaweb.gsfc.nasa.gov). The maps in Figure 1 are made with Natural Earth (Free vector and raster map data https://www.naturalearthdata.com).

Author contribution: NN suggested the event for the case-study, prepared ground-based data for preliminary analysis. NY developed software and performed data analysis. LB assisted with EISCAT data analysis and DL assisted with DMSP data analysis. DS provided Vostok data. The manuscript was prepared by NN and NY, after discussions with LB and DL.

Acknowledgements: The authors thank prof. V.A. Pilipenko for helpful discussions. The authors thank the institutes who maintain the IMAGE Magnetometer Array: Tromsø Geophysical Observatory of UiT the Arctic University of Norway (Norway), Finnish Meteorological Institute (Finland), Institute of Geophysics Polish Academy of Sciences (Poland), GFZ German Research Centre for Geosciences (Germany), Geological Survey of Sweden (Sweden), Swedish Institute of Space Physics (Sweden), Sodankylä Geophysical Observatory of the University of Oulu (Finland), and Polar Geophysical Institute (Russia). The results presented in this paper rely on data collected at magnetic observatories. The authors thank the national institutes that support them and INTERMAGNET for promoting high standards of magnetic observatory practice (www.intermagnet.org). The authors thank the Arctic and Antarctic Research Institute in Russia for providing ground magnetometer data from VOS station (http://geophys.aari.ru). The authors thank CDAWEB (https://cdaweb.gsfc.nasa.gov) for Cluster and OMNI data. EISCAT is an international association supported by research organisations in China (CRIRP), Finland (SA), Japan (NIPR and ISEE), Norway (NFR), Sweden (VR), and the United Kingdom (UKRI). This research was partly funded by the PolarProg and INTPART research programs under the Research Council of Norway (project numbers 246725 and 309135, NN, LB, DL) and by RFBR grant # 20-05-00787 A (NY).

The authors declare that they have no conflict of interest.

References

Akasofu, S.: Auroral Substorms: Search for Processes Causing the Expansion Phase in Terms of the Electric Current Approach, Space Sci. Rev., 212, 341–381, doi:10.1007/s11214-017-0363-7, 2017.

Balogh, A., Dunlop, M. W., Cowley, S. W. H., Southwood, D. J., Thomlinson, J. G., Glassmeier, K. H., Musmann, G., LÜHR, H., Buchert, S., AcuÑA, M. H., Fairfield, D. H., Slavin, J. A., Riedler, W., Schwingenschuh K., and Kivelson, M. G.: The Cluster Magnetic Field Investigation. *Space Sci. Rev.,* 79, 65–91, doi.:10.1023/A:1004970907748, 1997

Bland, E. C., and McDonald, A. J.: High spatial resolution radar observations of ultralow frequency waves in the southern polar cap, J. Geophys. Res. Space Physics, 121, 4005–4016, doi:10.1002/2015JA022235, 2016.

Fraser-Smith, A.C.: ULF/Lower-ELF Electromagnetic Field Measurements in the Polar Caps, Reviews of Geophysics and Space Physics, 29, 3, 497-512, doi:10.1029/RG020i003p00497, 1982

Kepko, L., Spence, H. E., and Singer, H. J.: ULF waves in the solar wind as direct drivers of magnetospheric pulsations, Geophys. Res. Lett., 29, 1197, doi:10.1029/2001GL014405, 2002.

https://doi.org/10.5194/angeo-2020-65
Preprint. Discussion started: 12 October 2020

Lepidi, S., Villante, U., Vellante, M., Palangio, P., and Meloni, A.: High resolution geomagnetic field observations at Terra Nova Bay, Antarctica, Ann. Geofis., 39, 519– 528, doi:10.4401/ag-3987, 1996.

Pilipenko, V.A., Kawano, H., and Mann, I.R.: Hodograph method to estimate the latitudinal profile of the field-line resonance frequency using the data from two ground magnetometers. Earth Planet Sp 65, 5, doi:10.5047/eps.2013.02.007, 2013

Yagova, N. V., Pilipenko, V. A., Lanzerotti, L. J., Engebretson, M. J., Rodger, A. S., Lepidi, S., and Papitashvili, V. O., Two-dimensional structure of long-period pulsations at polar latitudes in Antarctica, J. Geophys. Res., 109, A03222, doi:10.1029/2003JA010166, 2004

Yagova, N., Nosikova, N., Baddeley, L., Kozyreva, O., Lorentzen, D. A., Pilipenko, V., and Johnsen, M. G.: Non-triggered auroral substorms and long-period (1–4 mHz) geomagnetic and auroral luminosity pulsations in the polar cap, Ann. Geophys., 35, 365–376, doi:10.5194/angeo-35-365-2017, 2017.

Wing, S., Sibeck, D. G., Wiltberger, M., and Singer, H.: Geosynchronous magnetic field temporal response to solar wind and IMF variations, J. Geophys. Res., 107(A8), 1–10, doi:10.1029/2001JA009156, 2002.

Table 1. Station coordinates and their parameters

Station code	Geographic		Geomagnetic (CGM)		UT of MLT midnight
	Latitude	Longitude	Latitude	Longitude	
NAL	78.92	11.95	76.34	110.45	20:59
LYR	78.20	15.82	75.40	111.20	20:55
HOP	76.5	25.1	73.22	114.53	20:40
TRO	69.66	18.95	66.75	102.42	21:26
THL	77.48	290.83	84.84	29.19	3:13
DRV	-66.66	140.01	-80.37	236.04	12:55
VOS	-78.46	106.82	-83.57	55.15	1:02
DVS	-68.58	77.97	-74.75	101.17	21:58

https://doi.org/10.5194/angeo-2020-65
Preprint. Discussion started: 12 October 2020

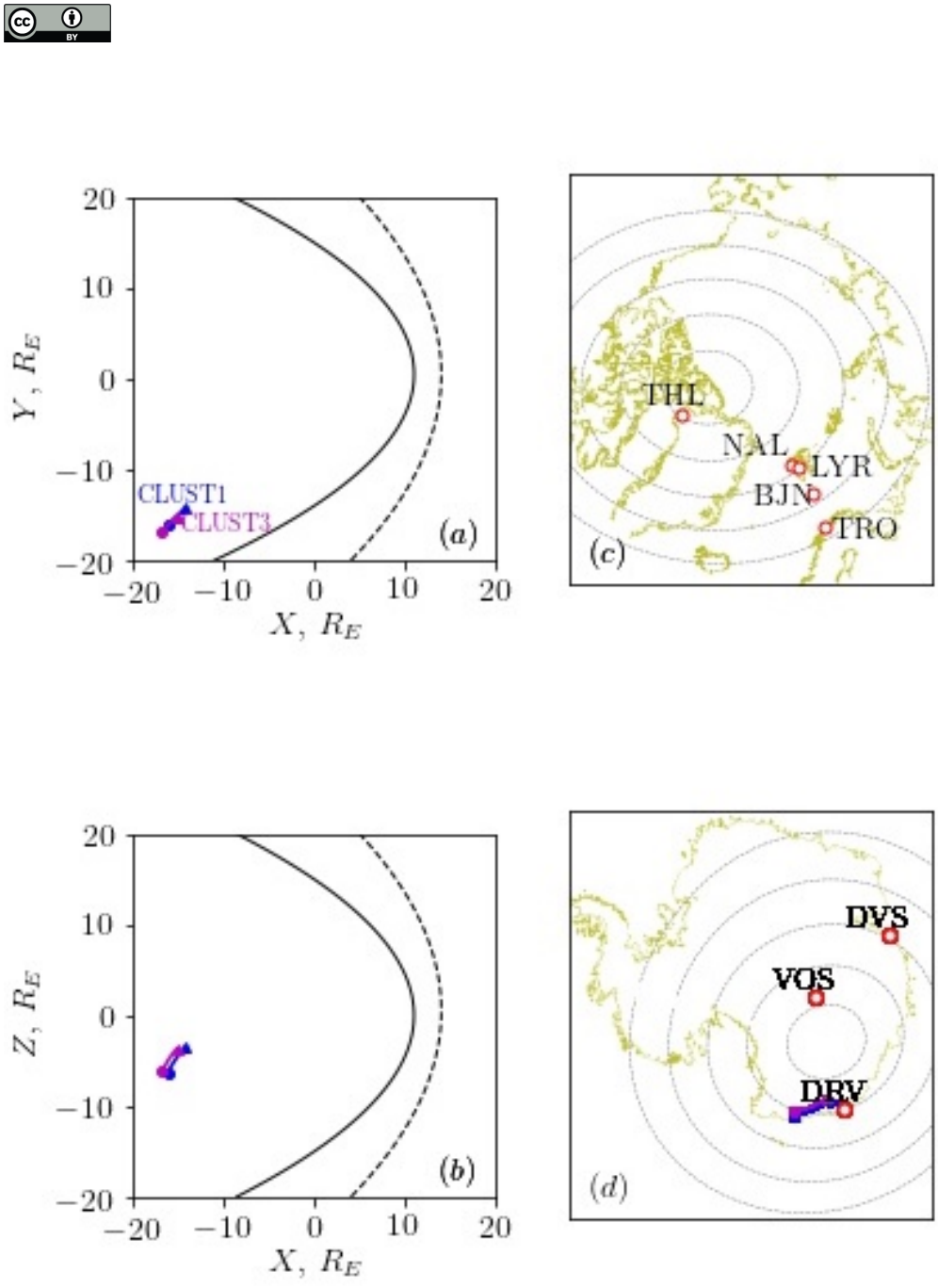

Figure 1: Cluster 1 and 3 satellites orbits in GSE coordinates (XY – panel (a), XZ –(b)) and their projection on the map with observatories located in the Northern (c) and Southern (d) hemispheres. Initial point and final point are marked with a circle and a triangle, respectively.

https://doi.org/10.5194/angeo-2020-65
Preprint. Discussion started: 12 October 2020

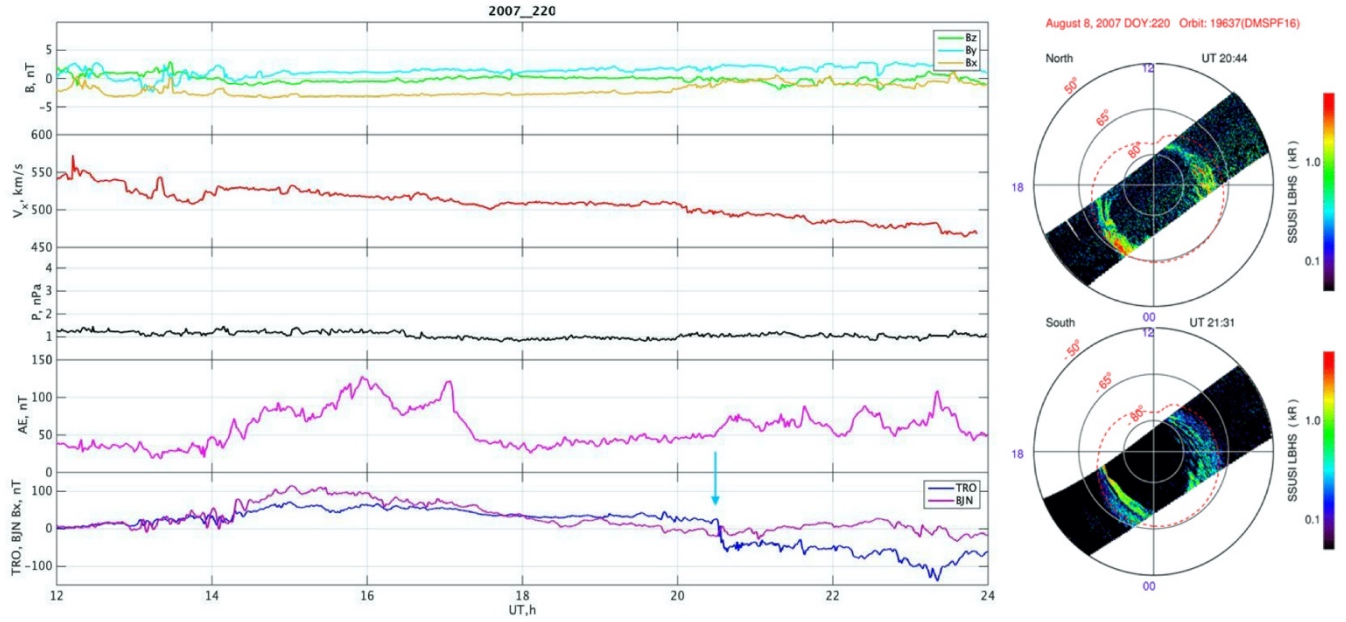

Figure 2: The particle precipitation seen from the DMSP satellite (right panel) and the solar wind parameters as well as ground based magnetometers data (left panel, from top to bottom: IMF all components; SW speed; SW pressure; AE-index; the magnetic field data from the TRO and BJN stations. The studied substorm is marked with the vertical blue arrow).

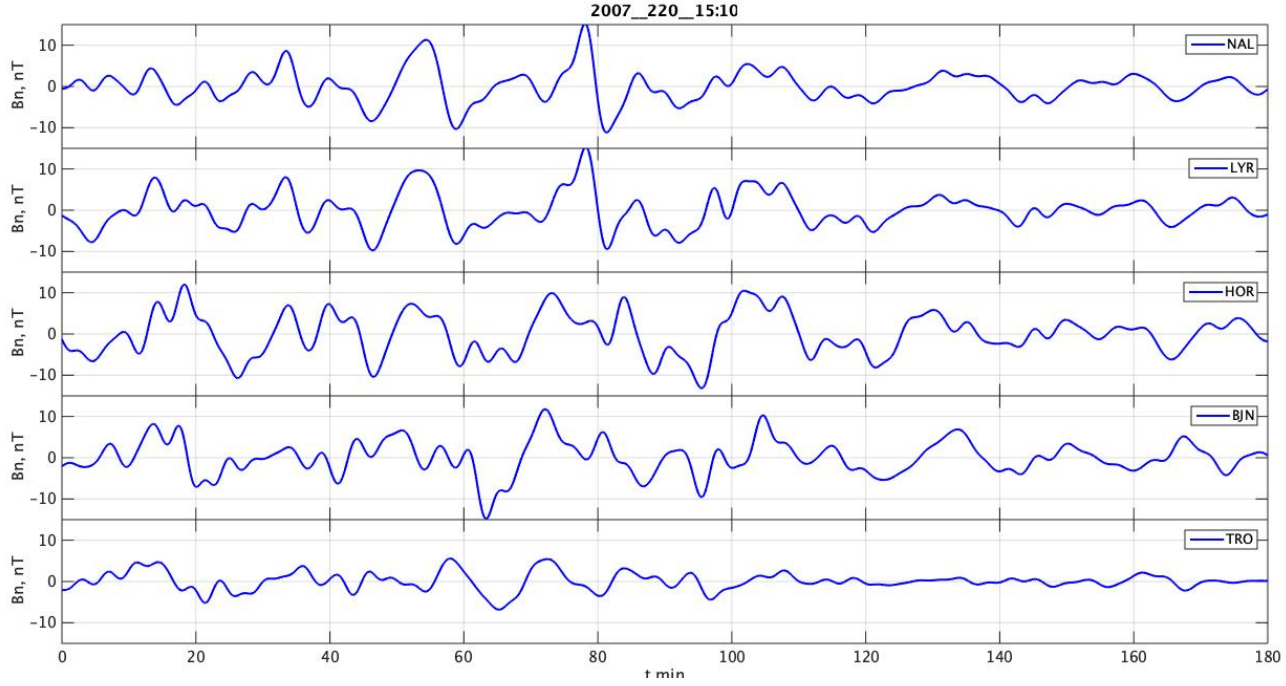

Figure 3: A latitude profile of geomagnetic pulsations registered on Svalbard (4 top panels) and at Tromsø (the bottom panel).

https://doi.org/10.5194/angeo-2020-65
Preprint. Discussion started: 12 October 2020

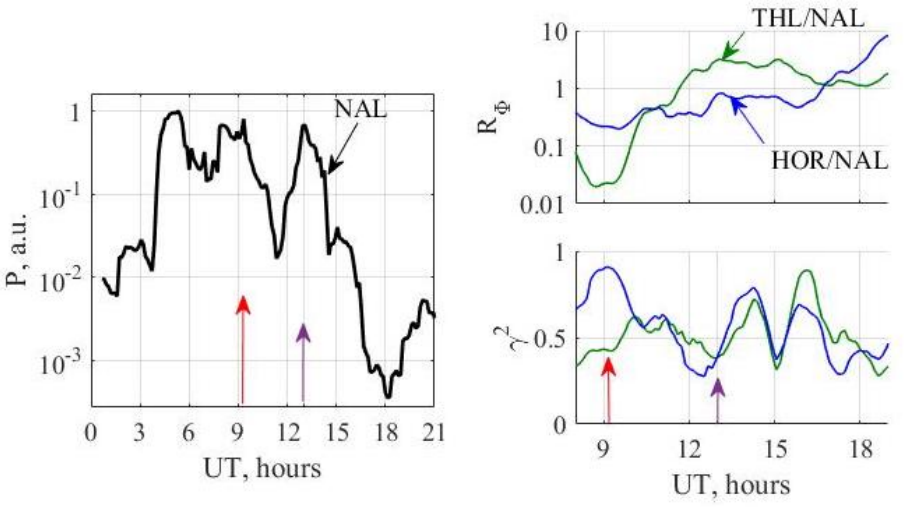

Figure 4: Diurnal variations of the spectral power in 1.2-1,9 mHz frequency band for NAL B_N component (a), PSD spectral ratio (b), and spectral coherence for the NAL-THL and NAL-HOR station pairs. Near-noon and afternoon maxima are marked by arrows.

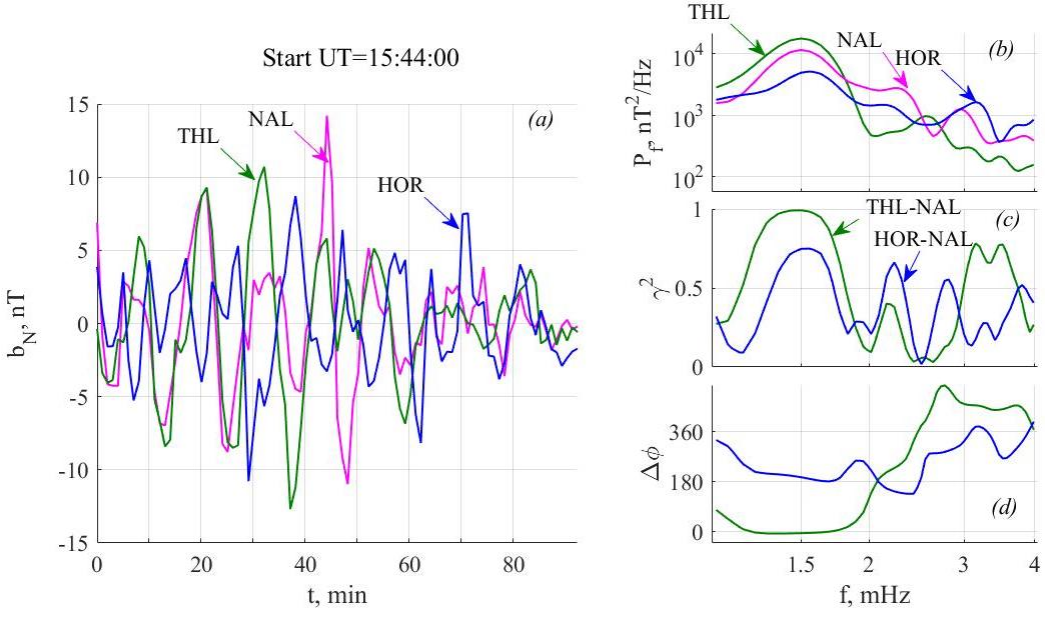

Figure 5: Pulsations of b_N component at NAL, THL, and HOR during the 1.5 hour interval starting at 15:44 UT (a); PSD spectra (b); spectral coherence for THL- NAL and HOR- NAL pairs of stations (c); phase differences (d). THL- NAL and HOR- NAL station pairs at panels (c) and (d) are shown with the same colours as THL and HOR at panels (a) and (b).

https://doi.org/10.5194/angeo-2020-65
Preprint. Discussion started: 12 October 2020

Annales Geophysicae Discussions

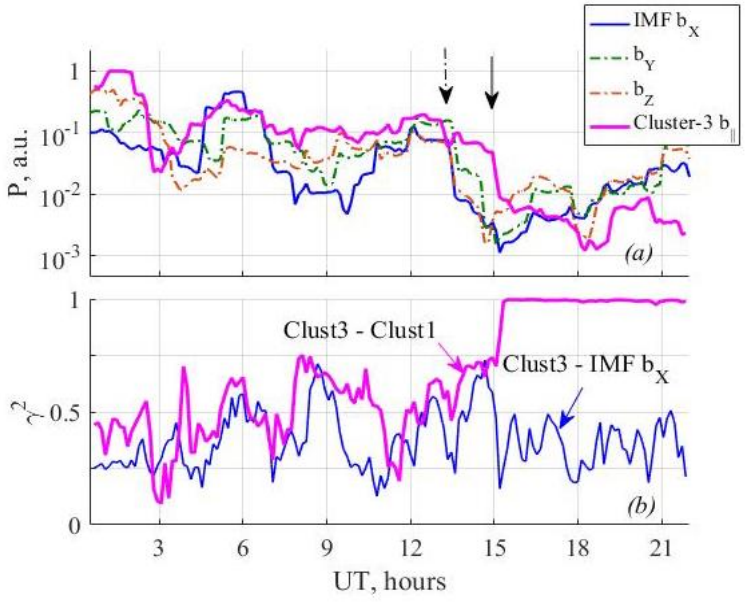

Figure 6: Diurnal variations of total spectral power (a) and average spectral coherence (b) for the three IMF components (GSM) and field aligned $b_{||}$ components at Clusters 1 and 3. Time instants of decrease of spectral power of IMF fluctuations and pulsations in $b_{||}$ at Cluster are marked with dot-dash and solid arrows, respectively.

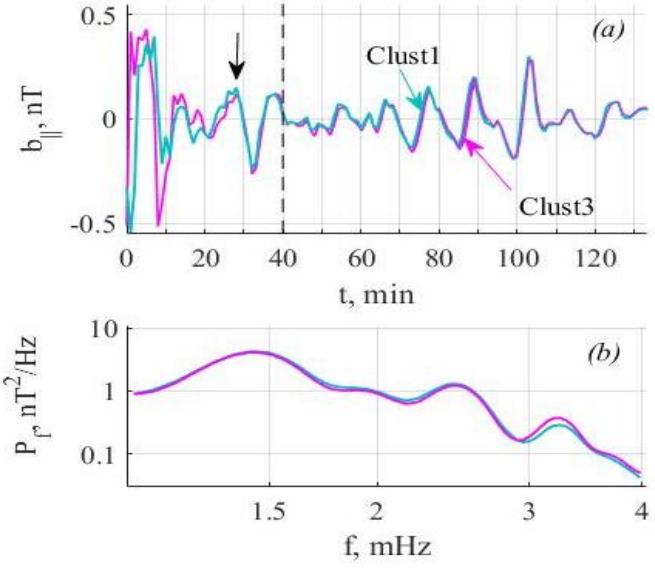

Figure 7: Pulsations of $b_{||}$ component in the magnetotail, recorded by Clusters 1 and 3 during the 1.5 hour intervals starting at 15:04 UT (a); 15:44 (b), and PSD spectra for the last interval (c). Change of pulsation regime is marked with an arrow and the start instant of the window, for which the spectra are calculated is given with a vertical dashed line. Pulsations at Clusters 1 and 3 are shown with the same colours in all the panels

https://doi.org/10.5194/angeo-2020-65
Preprint. Discussion started: 12 October 2020

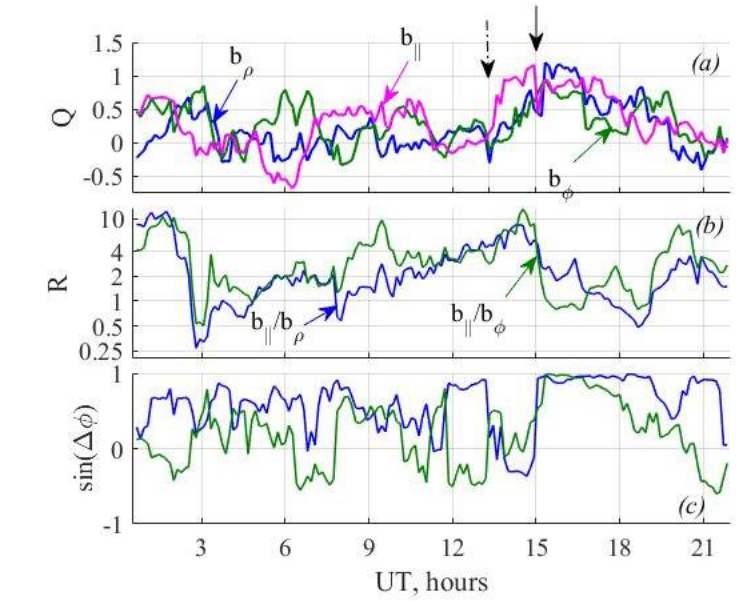

385

Figure 8: Time variations of the parameter Q (a), spectral field-aligned to transversal components spectral power ratio R (b), and a sign of phase difference (c) at Cluster 3. The change of pulsation regime in IMF and in $b_{\|}$ at Cluster at 15 UT is marked by the arrows, similar to Figures 7.

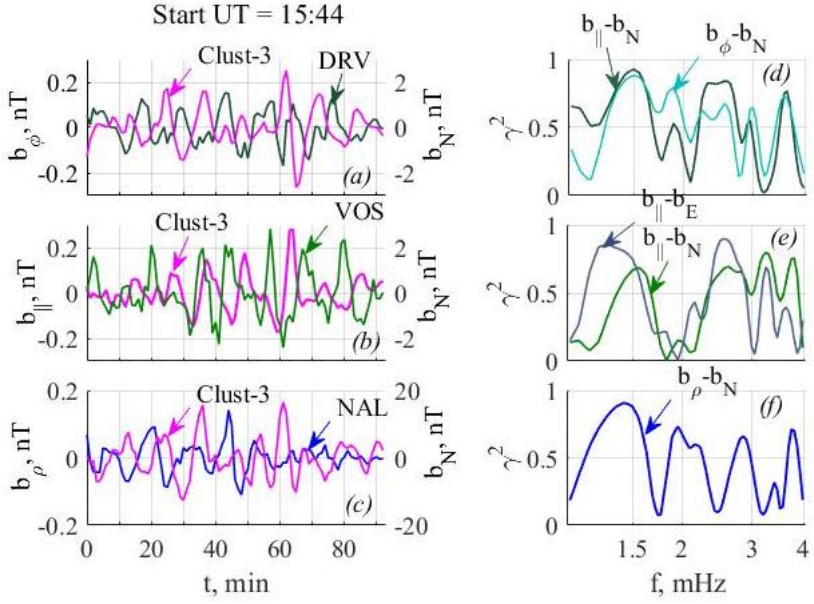

390 **Figure 9: Pulsations in the magnetotail (Cluster-3) and of b_N on Earth. Pulsations at Cluster 3 and one of the ground stations are shown in panels (a-c). A component with the maximal coherence at the f1 frequency with the corresponding station is shown at each of a-c panels. Left/right Y-axis correspond to Cluster 3/ground, respectively. Spectral coherence for the same satellite –station pairs are given in panels (d-f).**

https://doi.org/10.5194/angeo-2020-65
Preprint. Discussion started: 12 October 2020

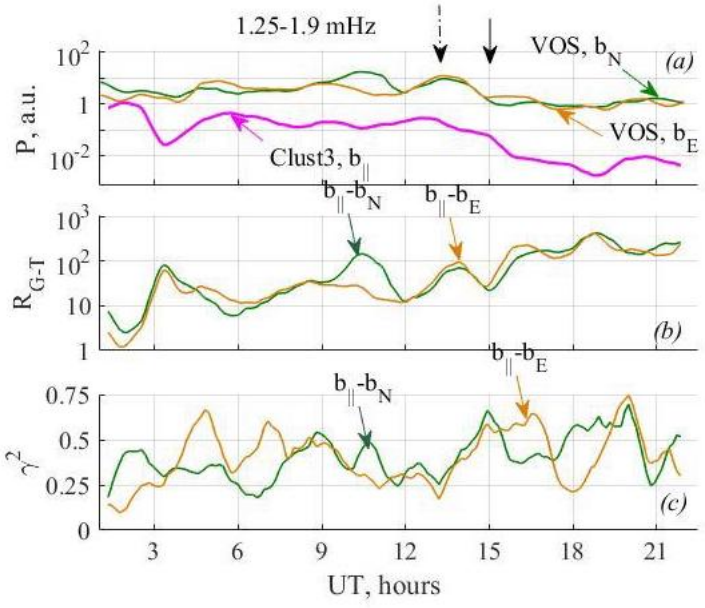

395 **Figure 10: Time variations of spectral power (*a*), ground to tail spectral ratio $R_{G\text{-}T}$ (b), and average spectral coherence (*c*) and in 1.2-1.9 mHz frequency band for $b_{||}$ components at Cluster 3 and both horizontal components at VOS. Time instants of decrease of spectral power of IMF fluctuations and pulsations in $b_{||}$ at Cluster are marked with dot-dash and solid arrows, respectively.**

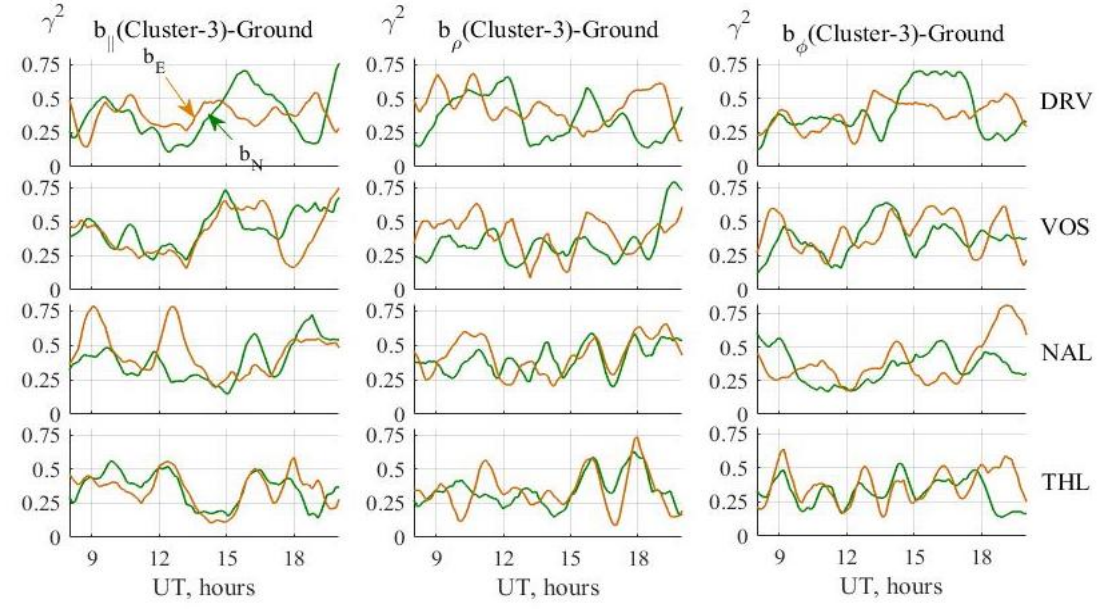

400 **Figure 11: Time variations of average spectral coherence in 1.2-1.9 mHz frequency band s for all component pairs formed from Cluster-3 and the 4 stations. 3 columns correspond to $b_{||}$, b_{ρ}, and b_{φ} Cluster components, and the rows show the DRV, VOS, NAL, and THL stations. The b_N and b_E components on Earth are shown in green and orange, respectively.**

https://doi.org/10.5194/angeo-2020-65
Preprint. Discussion started: 12 October 2020

Annales Geophysicae Discussions

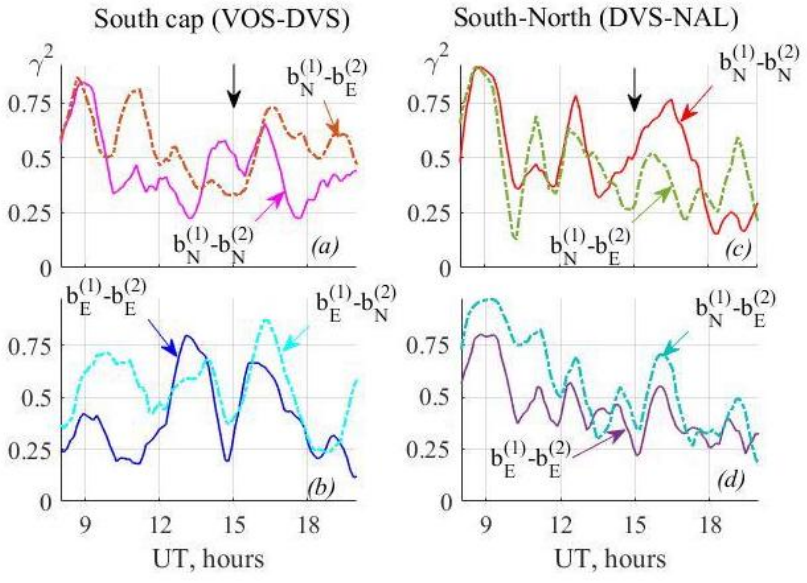

Figure 12: Time variations of average spectral coherence in 1.2-1.9 mHz frequency band between two points in the Southern polar cap and between the Southern and the Northern polar cap stations: (*a*) b_N component at VOS - both horizontal components at DVS; (b) b_E component at VOS - both horizontal components at DVS; (*c*) b_N component at DVS - both horizontal components at NAL; (*d*) b_E component at DVS - both horizontal components at NAL. Coherence for corresponding components (NN and EE) is shown in all the panels with solid lines, and cross-component (NE and EN) coherence is shown with dash-dot lines. Upper indexes indicated the number of a station in the station pair. Time instant of decrease of spectral power of pulsations at Cluster are marked with an arrow.

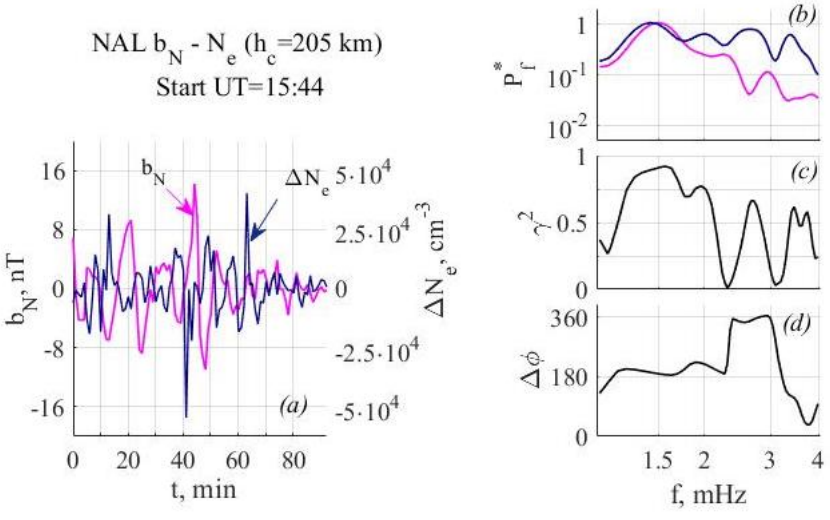

Figure 13: Pulsations of b_N component at NAL and fluctuations of N_e in the altitude band 190-220 km during the 1.5 hour interval starting at 15:44 UT (a); PSD spectra (b); spectral coherence (c); phase differences (d).

https://doi.org/10.5194/angeo-2020-65
Preprint. Discussion started: 12 October 2020

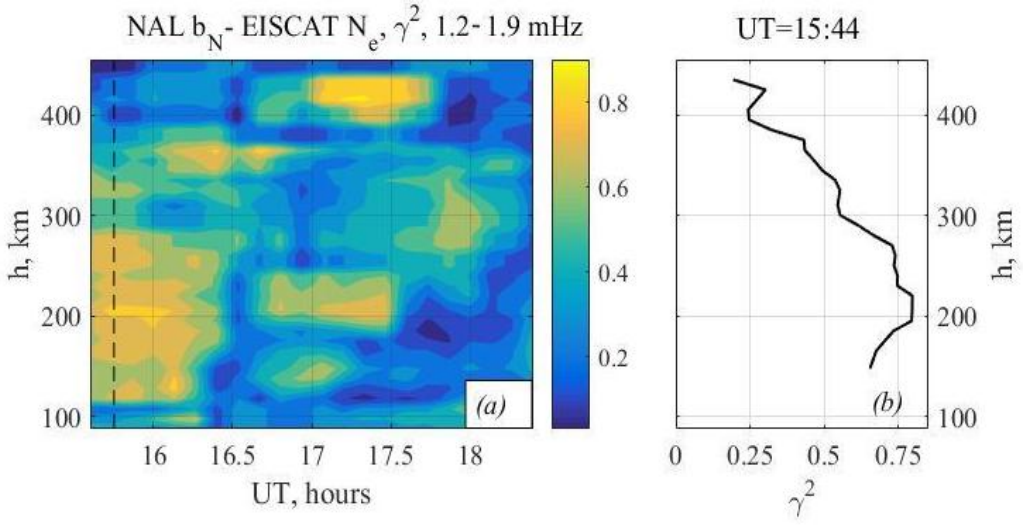

Figure 14: Dynamic altitude distribution of spectral coherence between EISCAT N_e and NAL b_N in 1.2-1.9 mHz frequency band at evening hours (a), and the altitude distribution of spectral coherence for the 15:44 interval.

415